Nonlinear Analysis and Control of Interleaved Boost Converter Using Real-Time Cycle to Cycle Variable Slope Compensation

Haimeng Wu, *Member, IEEE*, Volker Pickert, *Member, IEEE*, Damian Giaouris, *Member, IEEE*, and Bing Ji, *Member, IEEE*

***Abstract*—Switched-mode power converters are inherently nonlinear and piecewise smooth systems that may exhibit a series of undesirable operations that can greatly reduce the converter's efficiency and lifetime. This paper presents a nonlinear analysis technique to investigate the influence of system parameters on the stability of interleaved boost converters. In this approach, Monodromy matrix that contains all the comprehensive information of converter parameters and control loop can be employed to fully reveal and understand the inherent nonlinear dynamics of interleaved boost converters, including the interaction effect of switching operation. Thereby not only the boundary conditions but also the relationship between stability margin and the parameters given can be intuitively studied by the eigenvalues of this matrix. Furthermore, by employing the knowledge gained from this analysis, a real-time cycle to cycle variable slope compensation method is proposed to guarantee a satisfactory performance of the converter with an extended range of stable operation. Outcomes show that systems can regain stability by applying the proposed method within a few time periods of switching cycles. The numerical and analytical results validate the theoretical analysis, and experimental results verify the effectiveness of the proposed approach.**

***Index Terms*—Bifurcation control, interleaved boost converter, monodromy matrix, nonlinear analysis, variable slope compensation (VSC).**

I. Introduction

DUE to the benefits of current ripple cancellation, passive components size reduction, and improved dynamic response contributed by interleaving techniques [1]–[3], interleaved switch-mode power converters are widely used in power systems such as electric vehicles [4], photovoltaics power generation [5], and thermoelectric generator systems [6]. However, in spite of the widespread applications of this type of dc–dc converter, their nonlinear effects due to sequential switching operations have not been sufficiently considered in converter design.

In general, dc–dc converters are piecewise smooth systems and their dynamic operations show a manifestation of various nonlinear phenomena, as evidenced by sudden changes in operating region, bifurcation, and chaotic operation when some circuit parameters are varied [7], [8]. For example, it is possible to have a sudden increase in the current ripple and then it forces the converter to operate in forbidding current/voltage areas with adding low frequency, high amplitude components. These unexpected random-like behaviors potentially lead to a violation of designated operation contours, increased electromagnetic interference, reduced efficiency and in the worst case scenario a loss of control with consequent catastrophic failures. Unfortunately, all these phenomena cannot be predicted (and hence avoided) by using conventional linearized model of the converter. Without the thorough knowledge of the existing circuits, experience-based trial and error procedure are often applied in practice to restrain operating point within the safe operating region. As a result, circuit design criteria are always determined by selective ballpark values of components and parameters based on lessons learned from the past rather than applying an appropriate systematic design methodology.

A. Stability Analysis Methods for Power Converters

To study and analyze the inherent stability of power converters, most power electronics practitioners conventionally employ the linearized averaging technique to fit the analysis of power converter into the framework of linear systems theory, and thus discontinuities introduced by the switching action of the circuit are ignored [9], [10]. This gives a simple and accurate model for steady-state and dynamic response at timescale much slower than switching cycles but fails to encompass nonlinear behavior at a fast timescale as the switching action itself makes the converter model to be a highly nonlinear system.

Researchers had shown endeavor to develop the conventional averaging methodology and thus it was extended to frequency-dependent averaged models by taking into account of the effect of fast-scale dynamics [11]. A multifrequency averaging approach was then proposed to improve the conventional state-space averaging models [12], modeling the dynamic behavior

Manuscript received June 8, 2016; revised September 12, 2016; accepted October 24, 2016. Date of publication November 7, 2016; date of current version April 24, 2017. This work was supported in part by the Vehicle Electrical Systems Integration project (EP/I038543/1), which was funded by the Engineering and Physical Sciences Research Council, and in part by the scholarship from China Scholarship Council. Recommended for publication by Associate Editor P. S. Shenoy.

H. Wu, V. Pickert, and D. Giaouris are with the School of Electrical and Electronic Engineering, Newcastle University, Newcastle upon Tyne NE1 7RU U.K (e-mail: Haimeng.wu@ncl.ac.uk; Volker.pickert@ncl.ac.uk; Damian.Giaouris@ncl.ac.uk).

B. Ji is with the Department of Engineering, University of Leicester, Leicester LE1 U.K. (e-mail: Bing.ji@le.ac.uk).

Color versions of one or more of the figures in this paper are available online at http://ieeexplore.ieee.org.

Digital Object Identifier 10.1109/TPEL.2016.2626119

of dc–dc converters by applying and expanding the frequency-selective averaging method [13]. An analysis method based on the Krylov–Bogoliubov–Mitropolsky algorithm was developed to recover the ripple components of state variables from the averaged model [14]. However, such improved models have some limitations to describe chaotic dynamics completely and effectively. To address fast-scale nonlinearities, discrete nonlinear modeling is the most widely used approach. Nonlinear map-based modeling [15] developed from sampled-data modeling [16] in the early stages applies an iterative map for the analysis of system stability that is obtained by sampling the state variables of the converter synchronously with pulse width modulation (PWM) clock signals. This method is commonly referred to as the Poincaré map method. Stability is indicated by the eigenvalues of the fixed point of the Jacobian of the map, even though in some cases the map itself cannot be derived in closed form because of the transcendental form of the system's equations. Hence, the map has to be obtained numerically.

Other alternative approaches such as Floquet theory [17], Lyapunov-based methods [18], and trajectory sensitivity approach [19] are applied effectively for the nonlinear analysis of power converters. Specifically, the evolution of perturbation is studied directly in Floquet theory to predict the system's stability, by deriving the absolute value of the eigenvalues of the complete cycle solution matrices. In Lyapunov-based methods, piecewise linear Lyapunov functions are searched and constructed to describe the system's stability. For trajectory sensitivity approach, systems are linearized around a nominal trajectory rather than around an equilibrium point and the stability of the system can be determined by observing the change in a trajectory due to small initial or parameters variation. There have been combined approaches developed from combining state-space averaging and discrete modeling. Examples of these methods are design-oriented ripple-based approach [20], [21]; Takagi–Sugeno fuzzy model-based approach [22] and system-poles approach [23]. Apart from aforementioned approaches, other individual methods, such as symbolic approach [24] and energy balance model [25] were proposed to analyze the nonlinearities of switching power converters. A recent review paper on stability analysis methods for switching mode power converters has summarized some approaches presented [26].

B. Control of Nonlinearity in Power Converters

Various control techniques are proposed to tackle nonlinear behaviors based on the above methodologies, which can be classified into two categories: feedback-based and nonfeedback-based techniques. In the feedback-based group, a small time-dependent perturbation is tailored to make the system operation change from unstable periodic orbits (UPOs) to targeted periodic orbits. Ott–Grebogi–Yorke approach proposed by Ott *et al*. [27] was the first well-known chaos control method. One advantage of this method is that *a priori* analytical knowledge of the system dynamics is not required, which makes it easier to implement [28]. Then delayed feedback control methods were proposed to stabilize the UPOs in the field of nonlinear dynamics [29], [30]. In this method, the information of the current state and prior one-period state is used to generate signals for the stabilizing control algorithm. Washout filter-aided feedback control was proposed to address the Hopf bifurcation of dynamic systems [31]. Other filter-based noninvasive methods for the control of chaos in power converters have also been proposed [32]. Apart from the aforementioned control methods, a self-stable chaos-control method [33], predictive control [34] and frequency-domain approach [35] have been proposed to eliminate bifurcation and chaotic behavior in various switching dc–dc converters.

In the nonfeedback category, the control target is not set at the particular desired operating state, whereas the chaotic system can be converted to any periodic orbit. Resonant parametric perturbation is one of the most popular methods [36], [37]. In this approach, some parameters at appropriate frequencies and amplitude are normally perturbed to induce the system to stay in stable periodic regions, converting the system dynamic to a periodic orbit. Other examples of this type of method include the ramp compensation approach [38], fuzzy logic control [39], and weak periodic perturbation [40]. Compared to feedback-based methods, no online monitoring and processing are required in a nonfeedback approach, which makes it easy to implement and suitable for specific practical applications.

However, in spite of the various approaches available, the most interesting results are presented by abstract mathematical forms, which cannot be directly and effectively applied to the design of practical systems for industrial applications. In this paper, a relatively intuitional approach using Monodromy matrix is applied to investigate the system stability and design the advanced controller of interleaved boost converter. This Monodromy matrix contains all the comprehensive system information including the system parameters, external conditions, and coefficients of the controller [41], [42]. Accordingly, the influence of various parameters on overall system stability can be investigated intuitively and it is able to be used for the further study on interaction effect of the switching operation to system's behavior. Most importantly, the boundary conditions of stable operation and the information of stability margin and the parameters given can be obtained by the eigenvalues of this matrix. Furthermore, based on the knowledge gained from this matrix, a novel real-time cycle to cycle variable slope compensation (VSC) method is proposed to stabilize the system, avoiding phenomena of subharmonic and chaotic operation. Theoretical analysis is validated numerically and experimentally to show the effectiveness of this proposed method. The rest of this paper is organized as follows. The fundamental principle of the stability analysis methodology employed and the corresponding derivation of matrices is presented in Section II. The study of the control loop and the concept of control approach proposed are illustrated in Section III. Simulation results and the related analysis are shown in Section IV and the experimental results of interleaved boost converter using mixed-signal controller are given in Section V. The final section summarizes the conclusions drawn from investigation and analysis.

II. Theoretical Principle and Matrix Derivation

A. Nonlinear Phenomena

Nonlinear phenomena can commonly be found in the analysis of power electronics converters. Fig. 1(a) shows experimental

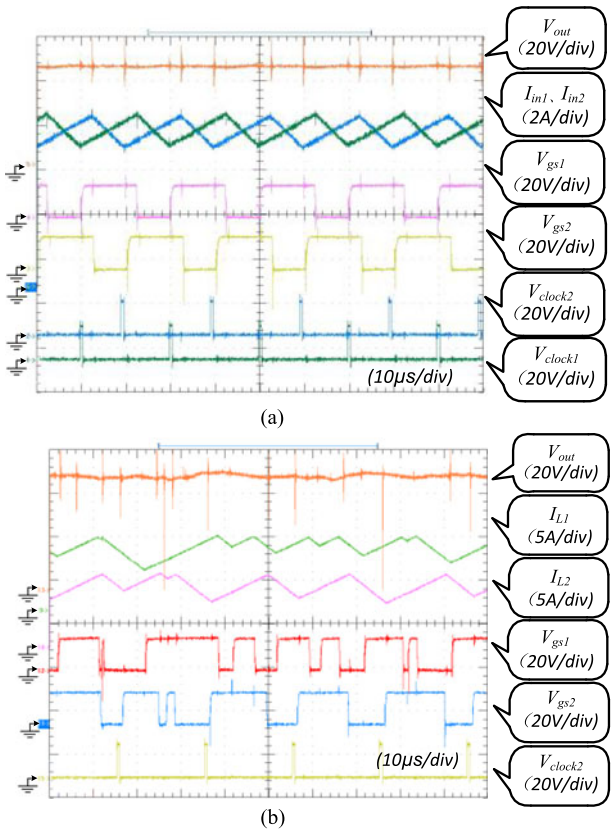

Fig. 1. Operation of interleaved boost converter at two different values of slope compensation: (a) Stable operation (period-1). (b) Chaotic operation.

TABLE I
SPECIFICATIONS OF SYSTEM PARAMETERS

Parameters	Value	Parameters	Value
Input voltage (V)	5∼18,	Frequency (kHz)	50
Output voltage (V)	24,	K_{iL}	1/8.5
Power rating (W)	60	K_{p1}	0.5
Inductance (μH)	75	K_{i1}	2000
Output capacitance (μF)	40	$m_c * T$	–0.10
K_{vc}	1/10		

results of an interleaved boost converter (circuit parameters are shown in Table I) when it is in the stable operation (period-1), in contrast, Fig. 1(b) presents its chaotic operation where the only difference is a slight change at the values of slope compensation. Thus, the stability analysis is crucial to guarantee the stable operation of the converter as the small variation of parameters may change the performance of converter dramatically. The study of how the value of slope compensation affects the stability of the system and its influence to the margin of system stability can be fully given by using the Monodromy matrix based method, which is presented in the following.

B. Concept of Monodromy Matrix Based Method

The topology of an interleaved boost converter and the diagram of a control strategy are shown in Fig. 2, K_i and K_p represent the gains of the PI controller; K_{vc} and K_{il} are the

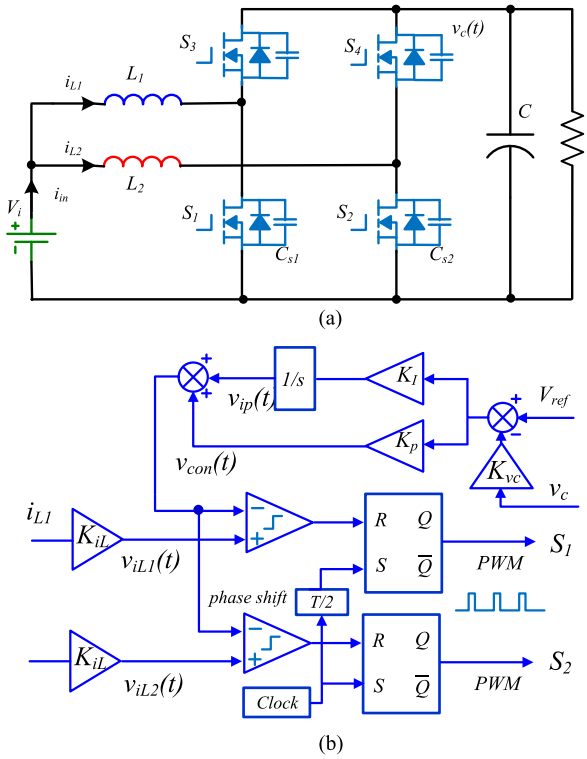

Fig. 2. (a) Topology of interleaved boost converter. (b) Diagram of control strategy for interleaved boost converter.

gain of signals from the practical sampled output voltage v_c and inductor currents i_{Li} $(i = 1, 2)$ to the controller, respectively. The inductor currents i_{L1} , i_{L2}, capacitor voltage v_c, and the output of the integrator in the feedback loop v_{ip} are chosen as the state variables. S_1 and S_2 are the switches employing the interleaving PWM control technique, which means that there is an 180° phase shift between them.

The key waveforms of the converter at different duty cycles in the steady-state operation are illustrated in Fig. 3(a) (when $d > 0.5$) and Fig. 3(b) (when $d < 0.5$), respectively. It can be seen that there are four subintervals in one period for both operational modes and the state transition matrix (STM) can be represented as $\phi_1 \sim \phi_4$. The system states at different switching sequences can be described by the following state equations:

$$\dot{x} = \begin{cases} ①\mathbf{A_1}x + \mathbf{B_1}E & \mathrm{S}_1 \text{ and } \mathrm{S}_2 \\ ②\mathbf{A}_2x + \mathbf{B}_2E & \mathrm{S}_1 \text{ on and } \mathrm{S}_2 \text{ off} \\ ③\mathbf{A}_3x + \mathbf{B}_3E & \mathrm{S}_1 \text{ off and } \mathrm{S}_2 \text{ on} \\ ④\mathbf{A}_4x + \mathbf{B}_4E & \mathrm{S}_1 \text{ and } \mathrm{S}_2 \text{ off} \end{cases}. \quad (1)$$

The concept of Monodromy matrix based method is to deduce the stability of a periodic solution by linearizing the system around the whole periodic orbit. This can be obtained by calculating the state transition matrices before and after each switching and the saltation matrix that describes the behaviors of the solution during switching. The derivation of this matrix is shown in Fig. 4, which demonstrates that perturbation evolves in one complete period through four different STM and four saltation matrices $\mathbf{S}$ in sequence.

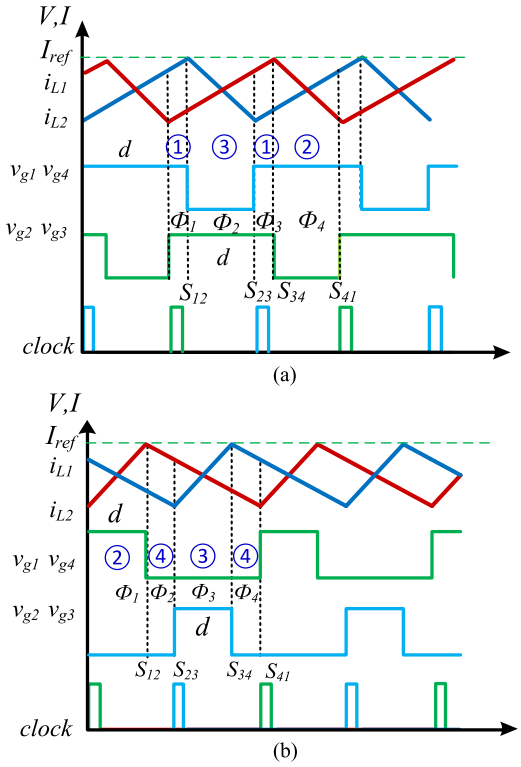

Fig. 3. (a) Key operational waveforms in steady state ($d > 0.5$). (b) Key operational waveforms in steady state ($d < 0.5$).

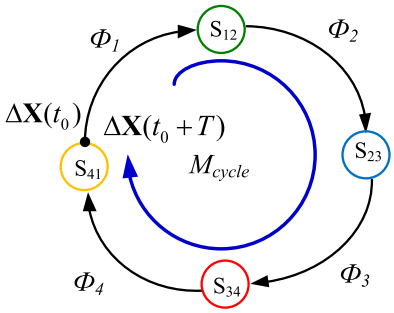

Fig. 4. Diagram of derivation of Monodromy matrix.

C. Theoretical Principle of Monodromy Matrix Based Method

The fundamental theory of this method is presented in the following. As shown in Fig. 5(a), assuming that a given system has an initial condition $\mathbf{x}(t_0)$ at time t_0 and it is perturbed to $\hat{\mathbf{x}}(t_0)$ such that the initial perturbation is $\Delta\mathbf{x}(t_0) = \mathbf{x}(t_0) - \hat{\mathbf{x}}(t_0)$. After the evolution of the original trajectory and the perturbed trajectory during time t, according to Floquet theory the perturbation at the end of the period can be related to the initial perturbation by

$$\Delta\mathbf{x}(t_0 + T) = \mathbf{\Phi}\,\Delta\mathbf{x}(t_0) \tag{2}$$

where $\mathbf{\Phi}$ is called the STM, which is a function of the initial state and time. For any power converter, the ON and OFF state of the switches makes the system evolve through different linear time-invariant (LTI) subsystems; therefore, for each subsystem, the STM can be obtained by the expression when the initial

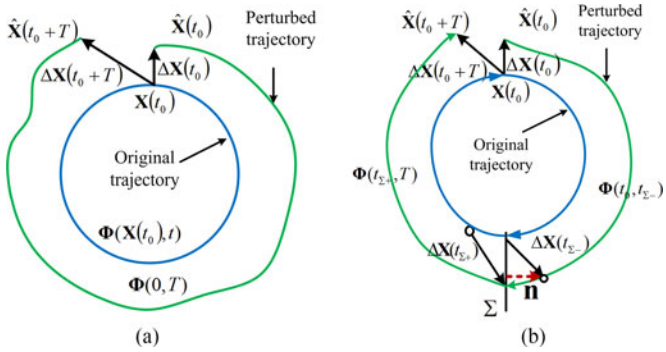

Fig. 5. Periodic solution and its perturbed solution.

conditions are given

$$\mathbf{\Phi} = e^{\mathbf{A}\,(t-t_0)} \tag{3}$$

where $\mathbf{A}$ is the state matrix that appears in the state equation

$$\dot{\mathbf{x}} = \mathbf{Ax}+\mathbf{Bu}. \tag{4}$$

In smooth systems, the fundamental matrix can be used to map the perturbation from the initial condition to the end of the period. Nevertheless, the vector field of a power electronics system is piecewise smooth and the vector field is discontinuous at the switching instant, which means that the STM cannot be utilized directly for stability analysis. As a result, some information representing the switching event needs to be introduced to fully describe the dynamic behavior of the system.

With the assumption that there is no jump in the state vector at switching instants, the Filippov method can be applied in the study of this discontinuous vector field, calculating the evolution of vectors during the interval of $[t_{\sum -},\, t_{\sum +}]$. The principle of this approach is illustrated in Fig. 5(b), and it describes the behavior of a perturbation crossing the switching surface Σ. Assuming that there is an initial perturbation $\Delta\mathbf{x}(t_0)$ at time of t_0, it then evolves to $\Delta\mathbf{x}(t_{\sum -})$, starting to cross the switching manifold at time of $t_{\sum -}$. After time $(t_{\sum +},\, t_{\sum -})$, it comes out of the switching surface and becomes $\Delta\mathbf{x}(t_{\sum +})$. The saltation matrix $\mathbf{S}$ is used to map the perturbation before and after the switching manifold as follows [43]:

$$\Delta\mathbf{x}(t_{\sum +}) = \mathbf{S}\,\Delta\mathbf{x}(t_{\sum -}) \tag{5}$$

$$\mathbf{S} = \mathbf{I} + \frac{(f_{\Sigma+} - f_{\Sigma-})\mathbf{n}^T}{\mathbf{n}^T f_{\Sigma-} + \frac{\partial h}{\partial t}} \tag{6}$$

where $\mathbf{I}$ is the identity matrix of the same order of state variables; h contains information of the switching condition; $\mathbf{n}$ represents the normal vector to the switching surface, and $f_{\sum -}$ and $f_{\sum +}$ are the differential equations before and after the switching instant. The derivations of (5) and (6) have been presented, in detail, in Appendix. Hence, the fundamental solution of a periodic system for one complete cycle, which is named the Monodromy matrix, can be represented as follows:

$$\mathbf{M} = \Phi(t_0, t_0 + T) = \Phi(t_{\Sigma+}, t_0 + T) \cdot \mathbf{S} \cdot \Phi(t_0, t_{\Sigma-}) \tag{7}$$

where $\Phi(t_0, t_{\sum -})$ and $\Phi(t_{\sum +}, t_0+\mathrm{T})$ are the state transition matrices in the time intervals of $[t_0, t_{\sum -}]$ and $[t_{\sum -}, t_0+\mathrm{T}]$, respectively. The eigenvalues of the Monodromy matrix (also termed the Floquet multipliers) can be applied to predict the stability. If all the eigenvalues have magnitudes less than unity, the system will be stable, otherwise, the system will exhibit various bifurcation and chaotic behaviors determined by the movement trajectory of crossing the unit circle.

D. Matrix Derivation

In the operation of interleaved boost converter as shown in Fig. 3, when the switches S_1 and S_2 are ON, the state equations can be expressed as

$$\frac{dv_c}{dt} = -\frac{v_c}{RC} \tag{8}$$

$$\frac{di_{L1}}{dt} = \frac{V_i}{L_1} \tag{9}$$

$$\frac{di_{L2}}{dt} = \frac{V_i}{L_2} \tag{10}$$

$$\frac{dv_{ipi}}{dt} = K_I(K_{vc}v_c - V_{\mathrm{ref}}) \tag{11}$$

When the switch S_1 is ON and S_2 is OFF, the state equations are

$$\frac{dv_c}{dt} = \frac{i_{L2}R - v_c}{RC} \tag{12}$$

$$\frac{di_{L1}}{dt} = \frac{V_i}{L_1} \tag{13}$$

$$\frac{di_{L2}}{dt} = \frac{V_i - v_c}{L_2} \tag{14}$$

$$\frac{dv_{ip}}{dt} = K_I(K_{vc}v_c - V_{\mathrm{ref}}). \tag{15}$$

When the switch S_1 is OFF and S_2 is ON, the state equations are

$$\frac{dv_c}{dt} = \frac{i_{L1}R - v_c}{RC} \tag{16}$$

$$\frac{di_{L1}}{dt} = \frac{V_i - v_c}{L_1} \tag{17}$$

$$\frac{di_{L2}}{dt} = \frac{V_i}{L_2} \tag{18}$$

$$\frac{dv_{ip}}{dt} = K_I(K_{vc}v_c - V_{\mathrm{ref}}). \tag{19}$$

When the switch S_1 and S_2 are OFF, the state equations are obtained as

$$\frac{dv_c}{dt} = \frac{(i_{L1} + i_{L2})R - v_c}{RC} \tag{20}$$

$$\frac{di_{L1}}{dt} = \frac{V_i - v_c}{L_1} \tag{21}$$

$$\frac{di_{L2}}{dt} = \frac{V_i - v_c}{L_2} \tag{22}$$

$$\frac{dv_{ipi}}{dt} = K_I(K_{vc}v_c - V_{\mathrm{ref}}). \tag{23}$$

The state equations above can be represented using vectors. Where x_1 is the capacitor voltage v_c, x_2 is the inductor current i_L, and x_3 the output of the integrator in the feedback loop v_{ip}, and the right-hand side state equations are expressed as

$$f_1 = \begin{bmatrix} -\frac{x_1}{RC} \\ \frac{V_i}{L_1} \\ \frac{V_i}{L_2} \\ K_I(K_{vc}x_1 - V_{\mathrm{ref}}) \end{bmatrix} \quad f_2 = \begin{bmatrix} \frac{x_3R - x_1}{RC} \\ \frac{V_i}{L_1} \\ \frac{V_i - x_1}{L_2} \\ K_I(K_{vc}x_1 - V_{\mathrm{ref}}) \end{bmatrix},$$

$$f_3 = \begin{bmatrix} \frac{x_2R - x_1}{RC} \\ \frac{V_i - x_1}{L_1} \\ \frac{V_i}{L_2} \\ K_I(K_{vc}x_1 - V_{\mathrm{ref}}) \end{bmatrix} \quad f_4 = \begin{bmatrix} \frac{(x_2 + x_3)R - x_1}{RC} \\ \frac{V_i - x_1}{L_1} \\ \frac{V_i - x_1}{L_2} \\ K_I(K_{vc}x_1 - V_{\mathrm{ref}}) \end{bmatrix}. \tag{24}$$

Thus, the corresponding state matrices for these four subintervals are shown in the following:

$$\mathbf{A}_1 = \begin{bmatrix} -\frac{1}{RC} & 0 & 0 & 0 \\ 0 & 0 & 0 & 0 \\ 0 & 0 & 0 & 0 \\ K_IK_{vc} & 0 & 0 & 0 \end{bmatrix} \tag{25}$$

$$\mathbf{A}_2 = \begin{bmatrix} -\frac{1}{RC} & 0 & \frac{1}{C} & 0 \\ 0 & 0 & 0 & 0 \\ -\frac{1}{L_2} & 0 & 0 & 0 \\ K_IK_{vc} & 0 & 0 & 0 \end{bmatrix} \tag{26}$$

$$\mathbf{A}_3 = \begin{bmatrix} -\frac{1}{RC} & \frac{1}{C} & 0 & 0 \\ -\frac{1}{L_1} & 0 & 0 & 0 \\ 0 & 0 & 0 & 0 \\ K_IK_{vc} & 0 & 0 & 0 \end{bmatrix} \tag{27}$$

$$\mathbf{A}_4 = \begin{bmatrix} -\frac{1}{RC} & \frac{1}{C} & \frac{1}{C} & 0 \\ -\frac{1}{L_1} & 0 & 0 & 0 \\ -\frac{1}{L_2} & 0 & 0 & 0 \\ K_IK_{vc} & 0 & 0 & 0 \end{bmatrix} \tag{28}$$

$$\mathbf{B_1} = \mathbf{B_2} = \mathbf{B_3} = \mathbf{B_4} = \begin{bmatrix} 0 & 0 & 0 & 0 \\ 0 & 0 & \frac{1}{L_1} & 0 \\ 0 & 0 & \frac{1}{L_2} & 0 \\ 0 & 0 & 0 & -K_I \end{bmatrix} \tag{29}$$

$$\mathbf{u} = \begin{bmatrix} 0 \\ 0 \\ V_i \\ V_{\text{ref}} \end{bmatrix}. \tag{30}$$

According to the control strategy of peak current control, the switching transients occur at the beginning of each switching period and the moment when the value of inductor current i_{Li} equals the reference signal. Therefore, the switching conditions from the ON to OFF state can be expressed as $h_i(x,t) = 0$ $(i = 12, 34)$,where

$$h_i(x,t) = K_p(V_{\text{ref}} - K_{vc}v_c) + v_{ip} - K_{iL}i_{Li}. \tag{31}$$

$$\mathbf{n}_{12} = \begin{bmatrix} \partial h_{12}/\partial x_1 \\ \partial h_{12}/\partial x_2 \\ \partial h_{12}/\partial x_3 \\ \partial h_{12}/\partial x_4 \end{bmatrix} = \begin{bmatrix} -K_pK_{vc} \\ -K_{iL} \\ 0 \\ 1 \end{bmatrix} \tag{32}$$

$$\mathbf{n}_{34} = \begin{bmatrix} \partial h_{34}/\partial x_1 \\ \partial h_{34}/\partial x_2 \\ \partial h_{34}/\partial x_3 \\ \partial h_{34}/\partial x_4 \end{bmatrix} = \begin{bmatrix} -K_pK_{vc} \\ 0 \\ -K_{iL} \\ 1 \end{bmatrix}. \tag{33}$$

The saltation matrices $\mathbf{S_{23}}$ and $\mathbf{S_{41}}$ turn out to be identity matrices, since they are related to the switching event from the OFF state to the ON state for S_1 and S_2 at the initial instant of every clock cycle, respectively, which means that the rising edge of the ramp causes the term of ∂ h/∂t in (5) to be infinity. When the duty cycle *d* is bigger than 0.5, the system states evolve from the following sequence as illustrated in Fig. 3(a):

①→ ③→ ①→ ②

Saltation matrix $\mathbf{S_{12a}}$ can be obtained as follows:

$$\mathbf{S}_{12\text{a}} = \begin{bmatrix} 1 - \frac{K_pK_{vc}x_3}{C(s_p+s_a)} & 0 & -\frac{K_{iL}x_3}{C(s_p+s_a)} & \frac{x_3}{C(s_p+s_a)} \\ 0 & 1 & 0 & 0 \\ \frac{K_pK_{vc}x_1}{L_2(s_p+s_a)} & 0 & 1+\frac{K_{iL}x_1}{L_2(s_p+s_a)} & -\frac{x_1}{L_2(s_p+s_a)} \\ 0 & 0 & 0 & 1 \end{bmatrix}. \tag{34}$$

Similarly, the saltation matrix $\mathbf{S}_{34\text{a}}$ can be derived as

$$\mathbf{S}_{34\text{a}} = \begin{bmatrix} 1 - \frac{K_pK_{vc}x_2}{C(s_p+s_a)} & -\frac{K_{iL}x_2}{C(s_p+s_a)} & 0 & \frac{x_2}{C(s_p+s_a)} \\ \frac{K_pK_{vc}x_1}{L_1(s_p+s_a)} & 1+\frac{K_{iL}x_1}{L_1(s_p+s_a)} & 0 & -\frac{x_1}{L_1(s_p+s_a)} \\ 0 & 0 & 1 & 0 \\ 0 & 0 & 0 & 1 \end{bmatrix} \tag{35}$$

where

$$s_p = \mathbf{n}_{34}^T f_{on} = \mathbf{n}_{34}^T f_1 = \frac{K_P K_{vc} x_1}{RC} - \frac{K_{iL}V_i}{L_2} + K_I(K_{vc}x_1 - V_{\text{ref}}) \tag{36}$$

$$s_a = \frac{\partial h}{\partial t} = 0. \tag{37}$$

For the interleaved control algorithm, the time of each subinterval can be represented in terms of *d* and *T*. The state transition matrices are given by the matrix exponential, hence

$$\begin{cases} \mathbf{\Phi}_1 = e^{\mathbf{A}_1 (d-0.5)T} \\ \mathbf{\Phi}_2 = e^{\mathbf{A}_3 (1-d)T} \\ \mathbf{\Phi}_3 = e^{\mathbf{A}_3 (d-0.5)T} \\ \mathbf{\Phi}_4 = e^{\mathbf{A}_2 (1-d)T} \end{cases}. \tag{38}$$

When duty cycle *d* is less than 0.5, the evolution of system states can be expressed in the following sequence:

②→ ④→ ③→ ④

Fig. 3(b) presents the key operational waveforms in steady state at this condition. The saltation matrices $\mathbf{S_{12b}}$ and $\mathbf{S_{34b}}$ can be calculated as follows:

$$\mathbf{S}_{12\text{b}} = \begin{bmatrix} 1 - \frac{K_pK_{vc}x_2}{C(s_p+s_a)} & -\frac{K_{iL}x_2}{C(s_p+s_a)} & 0 & \frac{x_2}{C(s_p+s_a)} \\ \frac{K_pK_{vc}x_1}{L_1(s_p+s_a)} & 1+\frac{K_{iL}x_1}{L_1(s_p+s_a)} & 0 & -\frac{x_1}{L_1(s_p+s_a)} \\ 0 & 0 & 1 & 0 \\ 0 & 0 & 0 & 1 \end{bmatrix} \tag{39}$$

$$\mathbf{S}_{34\text{b}} = \begin{bmatrix} 1 - \frac{K_pK_{vc}x_3}{C(s_p+s_a)} & 0 & -\frac{K_{iL}x_3}{C(s_p+s_a)} & \frac{x_3}{C(s_p+s_a)} \\ 0 & 1 & 0 & 0 \\ \frac{K_pK_{vc}x_1}{L_2(s_p+s_a)} & 0 & 1+\frac{K_{iL}x_1}{L_2(s_p+s_a)} & -\frac{x_1}{L_2(s_p+s_a)} \\ 0 & 0 & 0 & 1 \end{bmatrix} \tag{40}$$

where

$$s_p = \frac{-K_P K_{vc}(x_2 R - x_1)}{RC} - \frac{K_{iL}V_i}{L_1} + K_I(V_{\text{ref}} - K_{vc}v_c) \tag{41}$$

$$s_a = \frac{\partial h}{\partial t} = 0. \tag{42}$$

When duty cycle is less than 0.5, the state transition matrices are given as

$$\begin{cases} \mathbf{\Phi}_1 = e^{\mathbf{A}_2\, dT} \\ \mathbf{\Phi}_2 = e^{\mathbf{A}_4\,(0.5-d)T} \\ \mathbf{\Phi}_3 = e^{\mathbf{A}_3\, dT} \\ \mathbf{\Phi}_4 = e^{\mathbf{A}_4\,(0.5-d)T} \end{cases}. \tag{43}$$

Thus, the Monodromy matrix $\mathbf{M}$ can be calculated by the following expression:

$$\mathbf{M} = \mathbf{\Phi}_{\text{cycle}} = \mathbf{\Phi}_1 \times \mathbf{S}_{12} \times \mathbf{\Phi}_2 \times \mathbf{S}_{23} \times \mathbf{\Phi}_3 \times \mathbf{S}_{34} \times \mathbf{\Phi}_4 \times \mathbf{S}_{41}. \tag{44}$$

This contains all of the information about the system input and load conditions, the parameters of the converter and the coefficients of the control loop, and therefore the influence of any system parameter on system stability can be analyzed using this matrix.

III. Proposed Control Method

Slope compensation is widely adopted in many different kinds of converters employing peak current mode control to avoid unstable phenomenon when the duty cycle d is bigger than 0.5. However, although several papers mentioned different methods to calculate the minimum required value of the compensation ramp in order to sufficiently eliminate subharmonic oscillations [44], [45], the influence of the slope parameter m_c to the margin of system stability cannot be investigated theoretically in these methods. In the Monodromy matrix based approach, the slope parameter m_c can be introduced in the derived saltation matrices $\mathbf{S_{12}}$ and $\mathbf{S_{34}}$. Thus, the relationship among value of m_c, other variables and margin of stable operation can be intuitively demonstrated by using the locus of eigenvalues. Specifically, by altering various coefficients of the Monodromy matrix, the stability of the system will be influenced correspondingly. Based on this concept, a real-time VSC method is proposed to control the nonlinear behavior of power converters, which is illustrated in Fig. 6. The difference compared to conventional constant slope compensation is that the amplitude of compensation ramp a_c can be varying according to the change of external conditions, such as input and output voltage or load conditions.

When applying slope compensation to peak current control, the time derivative of the switching manifold changes by adding a variable slope signal to the switching manifold h, thus the switching condition becomes

$$h_i(x,t) = K_p(V_{\text{ref}} - K_{vc}v_c) + v_{ip} + m_c t - K_{iL} i_{Li}. \tag{45}$$

There is no effect on its normal vector, but compared to peak current control without slope compensation, the $\partial h/\partial t$ changes from 0 to

$$\frac{\partial h}{\partial t} = m_c = -\frac{a_c}{T_s}. \tag{46}$$

The diagram of proposed control strategy is shown in Fig. 6(a), information of the input voltage V_i, output voltage v_c, and the output of the PI controller are gathered as the input of the VSC control block. After the operation of calculation

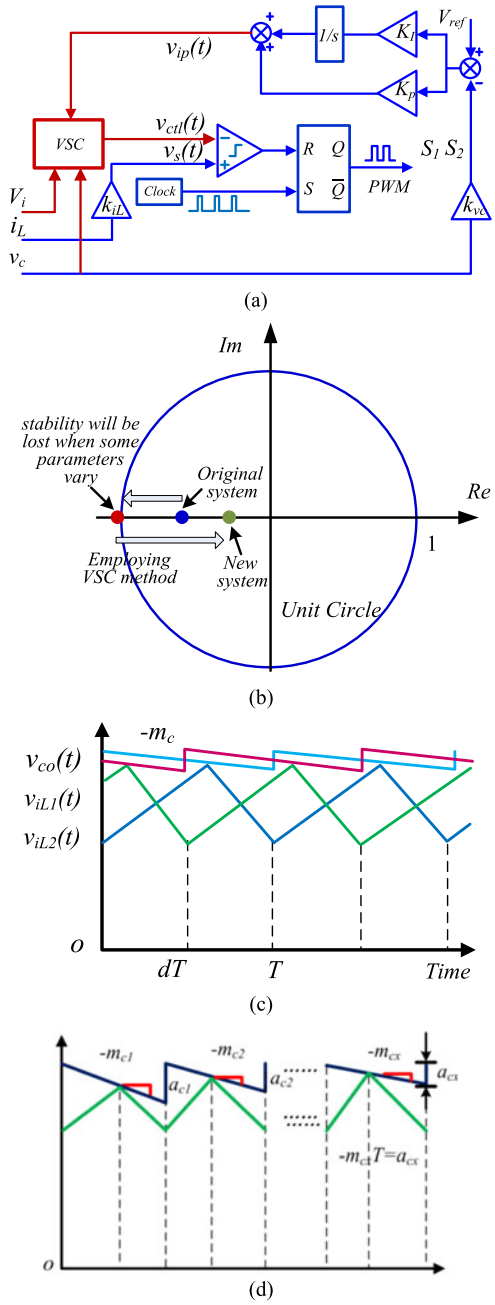

Fig. 6. (a). Diagram of proposed control strategy. (b) Movement of eigenvalues applying proposed method. (c) Conventional constant slope compensation in interleaved boost converters. (d) Proposed real-time VSC using Monodromy matrix.

in this control block, a control signal $v_{\text{ctrl}}(t)$ containing the slope compensation with appropriate amplitude can be generated as the input signal of PWM generation block. As illustrated in Fig. 6(b), the original system may lose the stability when some parameters are varying. Thus by choosing the appropriate parameter a_c in the new constructed Monodromy matrix, the corresponding eigenvalues can be located at any targeted place within the unit circle which indicates stable period-1 operation. In other words, for the given location of eigenvalues, the value of a_c can be calculated at every switching period accordingly, which is shown in Fig. 6(d). The proposed method is to keep

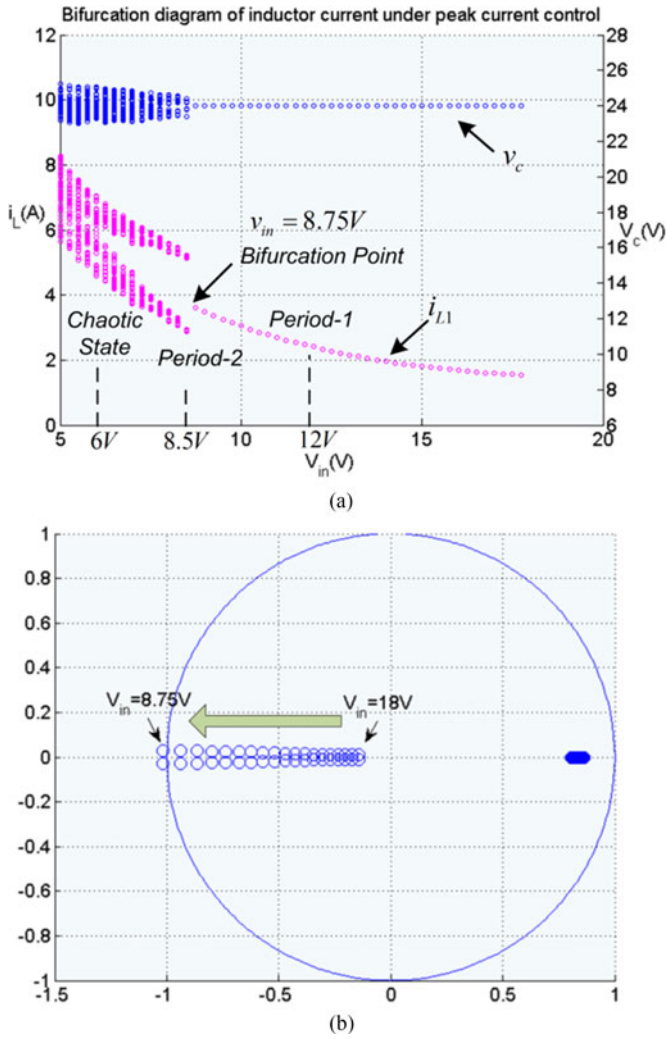

Fig. 7. (a). Bifurcation diagram of output voltage and inductor current at different input voltages. (b) Corresponding locus of eigenvalues.

the magnitude of the eigenvalues the same at different input voltages. For the controller design, the relationship between the input voltage and required value of a_c must be obtained. Therefore, the following nonlinear transcendental equation should be solved numerically: $|eig(\mathbf{M}(0,T))| = R$. Where R is the radius of the circle on which the eigenvalues of the Monodromy matrix lie.

IV. Simulation Results

The specifications of system parameters are presented in Table I. Simulation results are produced based on the models built in MATLAB/Simulink using these parameters above. Fig. 7(a) shows the bifurcation diagram of output voltage v_c and inductor current i_{L1} at different input voltages. The input voltage is varied from 5 to 18 V with constant amplitude of slope ($a_c = |m_{c*}\mathrm{T}| = 0.1$). It can be seen that the system experiences from chaotic state to double period (period-2) and eventually to stable period-1 operation with the increase of input voltages. The bifurcation phenomena take place when the input is set close to 8.75 V, where the system changes

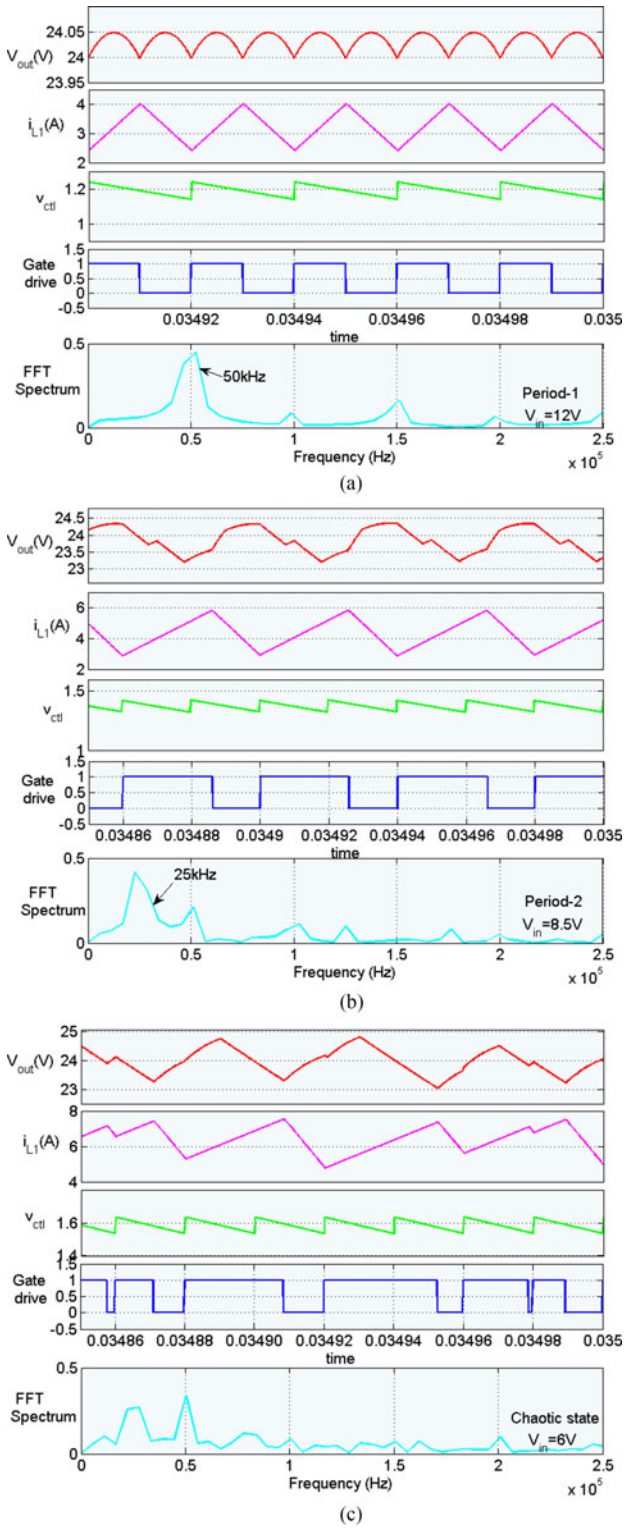

Fig. 8. Key operational waveforms and FFT spectrum at different operation states in simulation: (a) period-1; (b) period-2; (c) chaotic state.

between double-period oscillation and period-1 operation. The corresponding eigenvalues of system at different inputs can be calculated using the expression of Monodromy matrix derived and the movement track of eigenvalues at different inputs can be plotted, as shown in Fig. 7(b). The related

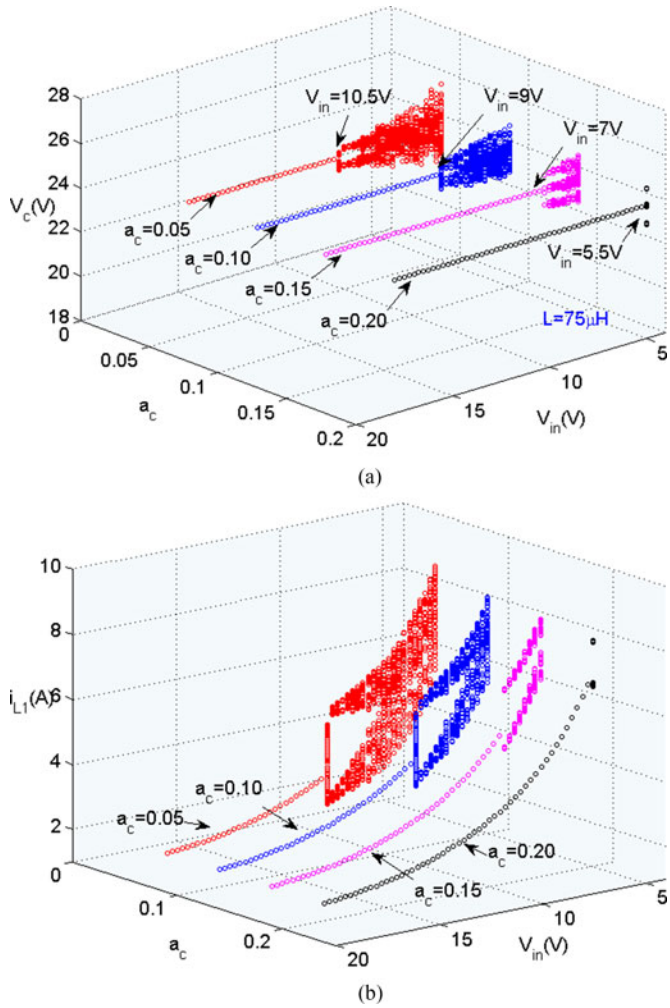

Fig. 9. Bifurcation diagram of inductor current and output voltage at different input voltages and ac in simulation: (a) output voltage; and (b) inductor current.

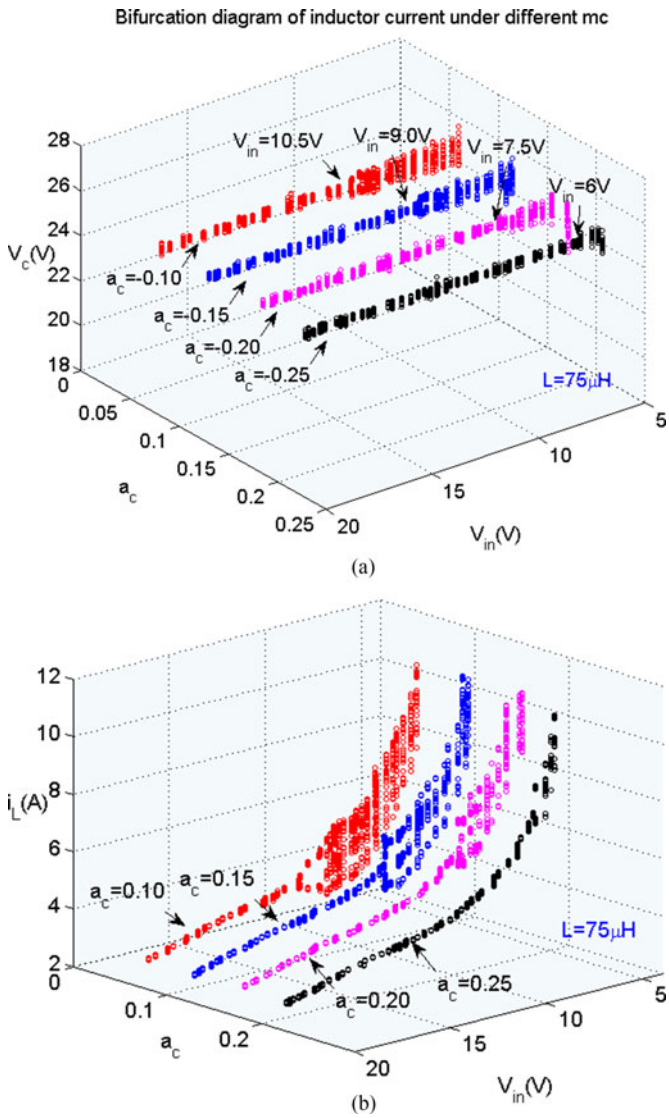

Fig. 10. Experimental bifurcation diagram of inductor current and output voltage at different input voltages and m_c: (a) output voltage; and (b) inductor current.

eigenvalues reach the border of unit circle when input voltage equals 8.75 V, which demonstrates the system will exhibit period doubling oscillation at this condition. The numerical computation matches with the simulation results well and the margin of system stability can be intuitively indicated by the locus of eigenvalues.

Key operational waveforms and fast Fourier transform (FFT) spectrum at different inputs (12, 8.5, and 6 V) are shown in Fig. 8(a), (b) and (c), respectively. The waveforms are output voltage v_c, inductor current of one phase i_{L1}, corresponding control signal $i_{\rm ctrl}$, generated PWM drive signal and FFT spectrum of drive signal from top to bottom. When input voltage equals 12 V, the system is to run at stable period 1, which is the expected operation region as shown in Fig. 7(a). When the input voltage is reduced to 8.5 V, the frequency of generate PWM reduces from 50 to 25 kHz according to the FFT spectrum. The nonperiodic and random-like waveforms demonstrate that the converter is to run at chaotic operation. We can see the ripple of voltage and current increase dramatically from period-1 to the chaotic operation through period 2. Specifically, the ripple voltage changes from nearly 0.05 to 1.7 V and ripple current varies from 1.5 to 3.2 A. Thus it is evident that the chaotic operation does cause more losses and degrade the performance of the converter.

In order to further study the relationship among $V_{\rm in}$, a_c and system stability, the bifurcation diagram of inductor current and output voltage at different input voltages and a_c are shown in Fig. 9. The amplitude of slope is set at 0.05–0.20 with the step of 0.05 and the bifurcation points varies from 10.5 to 5.5 V input when a_c is changed from 0.05 to 0.20 accordingly. It clearly shows the bifurcation points vary at different a_c, exhibiting certain linear relationship. The figure also shows that bigger amplitude of slope compensation brings in the wider range of stable operation at the same given input conditions. The Monodromy matrix can be expressed as a function $\mathbf{M}$ in terms of a_c and $V_{\rm in}$

$$\mathbf{M} = M(a_c, V_{\rm in}). \tag{47}$$

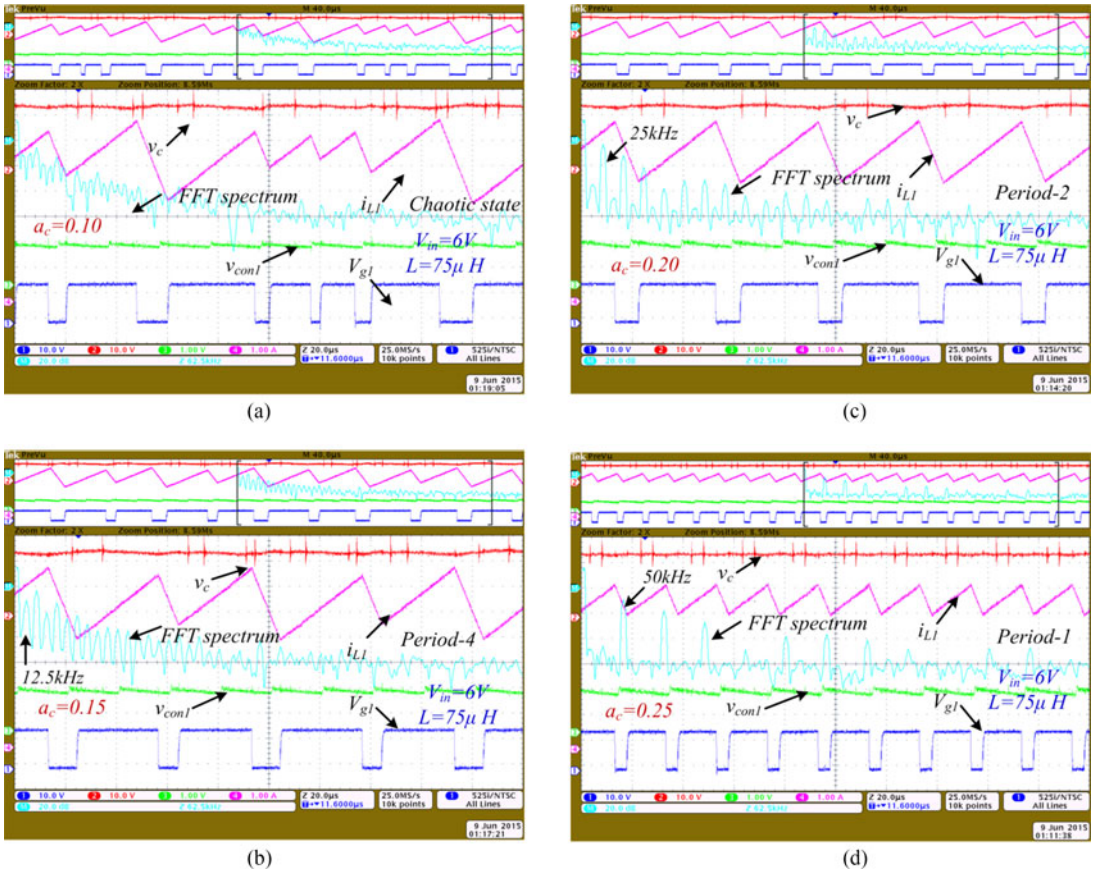

Fig. 11. Experimental results of key operational waveforms at different compensation slope: (a) $a_c = 0.10$; (b) $a_c = 0.15$ (c) $a_c = 0.20$; and (d) $a_c = 0.25$.

The border value of the stable operating region can be calculated using the Monodromy matrix derived, which provides the design guidance for the given system.

V. Experimental Verification

A. Bifurcation Diagram

To verify the analysis on simulation results, an interleaved boost converter with relevant control circuit have been designed using the specification presented in Table I. Fig. 10 presents the experimental bifurcation diagram of output voltage and inductor current at the conditions of different input voltages and values of a_c. Graphs are reconstructed based on the sampled and stored data, which are from the generated file by using Labview. Compared with the shown in Fig. 9, it can be seen that both waveforms are quite close but with some differences in terms of the practical values of a_c employed, profile and bifurcation point. The practical required value of a_c is slightly bigger (about 0.05) than the ones set in the simulation. Other differences are caused by the varying steps of input voltage in the experiment and the constant step setting in the simulation. The simulation results are from the ideal model-based calculation, and thus the sampled points generated for constant values are exactly located at one point. In contrast, errors in the experimental results are caused by the sampling resolution and quantization effect, and thus the constant values to sample will be transferred as values with some errors in the DSP controller. The errors are also related to settings of the zero-order hold and capture window in relevant registers, and this is normally set within a certain acceptable range to guarantee accuracy. In general, the simulation results are reliable enough so as to be used to facilitate the practical circuit design.

The influence of different value of a_c to the operation of converter is demonstrated in Fig. 11. The input voltage is set at 6 V, and a_c is set from 0.1 to 0.25 with the step of 0.05. Fig. 11(a) shows the converter is operated in the chaotic state when a_c equals 0.1; when the a_c is changed to 0.15, the FFT spectrum curve indicates the converter is in the operation of period-4, with the fundamental frequency of 12.5 kHz, which is a quarter of period-1. The operation of converter becomes to period-2 when a_c is set to 0.20, and stable operation of period-1 will occur if a_c is increased to 0.25. The key operation waveforms are presented in Fig. 11(b), (c), and (d), respectively. It is evident that the values of compensation ramp affect dramatically to the stability of converter's operation and the larger value of a_c can increase the stability of system.

B. Real-Time Cycle-to-Cycle VSC Control

In order to control nonlinear behavior and improve the performance of converters, an approach named real-time cycle-by-cycle VSC is proposed in this section, which is based on the knowledge of Monodromy matrix. The concept and principles

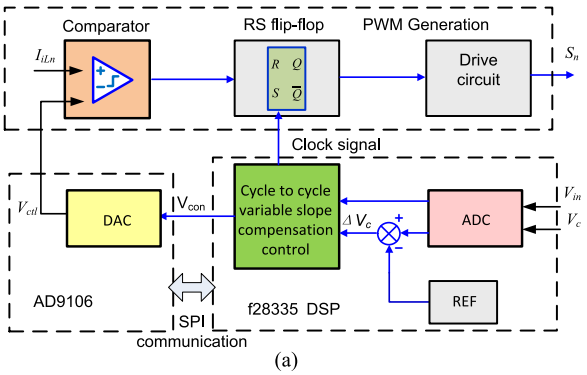

(a)

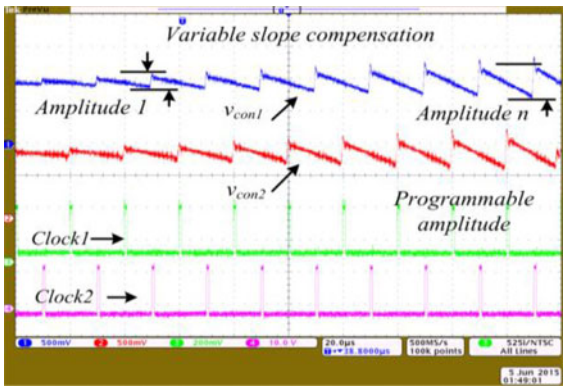

(b)

Fig. 12. Implementation of VSC control: (a) control strategy in the practical circuit; and (b) control and clock signals.

of this method are presented in Section III, but the challenge is the practical implantation of VSC. To address this problem, a high-performance digital to analogue (DAC) is employed with a DSP controller to achieve this advanced control method. As illustrated in Fig. 12(a), a TI F28335 based DSP controller is used as the core processor to achieve the functions of voltage signal sampling, calculation of control strategy, and sending commands to the external high-speed waveform generator AD9106 to produce the control signals. Two continuous time inductor currents are sampled and scaled by current sensors, and corresponding signals are fed into the comparators to generate the PWM signals. Fig. 13(b) presents the operational waveforms of control and clock signals, the upper waveforms are two current references added by variable slope compensations with a 180° shift, which are generated by this programmable DAC, and the bottom waveforms are the corresponding clock signals. The amplitudes of the slopes are programmed to increase within a given step to demonstrate the capability of cycle-by-cycle slope control.

As discussed in Section III, the eigenvalues of Monodromy matrix can be used to predict the bifurcation points of the system and the locus of eigenvalues can indicate the margin of the stable range at different levels of variation in system parameters or external input and output conditions. In other words, if a specific margin is set, the corresponding compensation slope can be calculated by the given parameters. Here, if the eigenvalues are placed at the radius of 0.5 in the unit circle, for example,

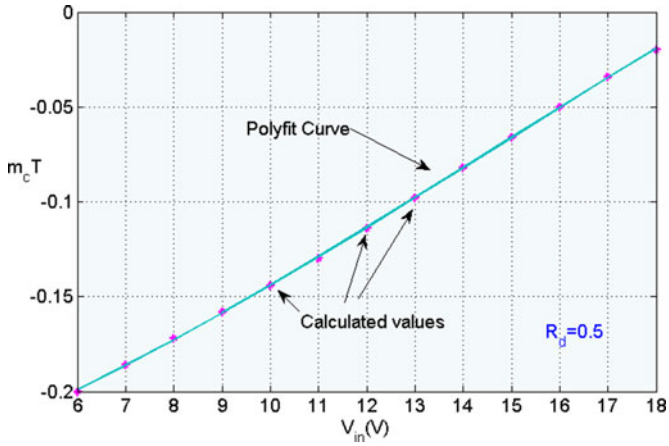

Fig. 13. Polyfit curve and calculated values of mc vs. input voltage.

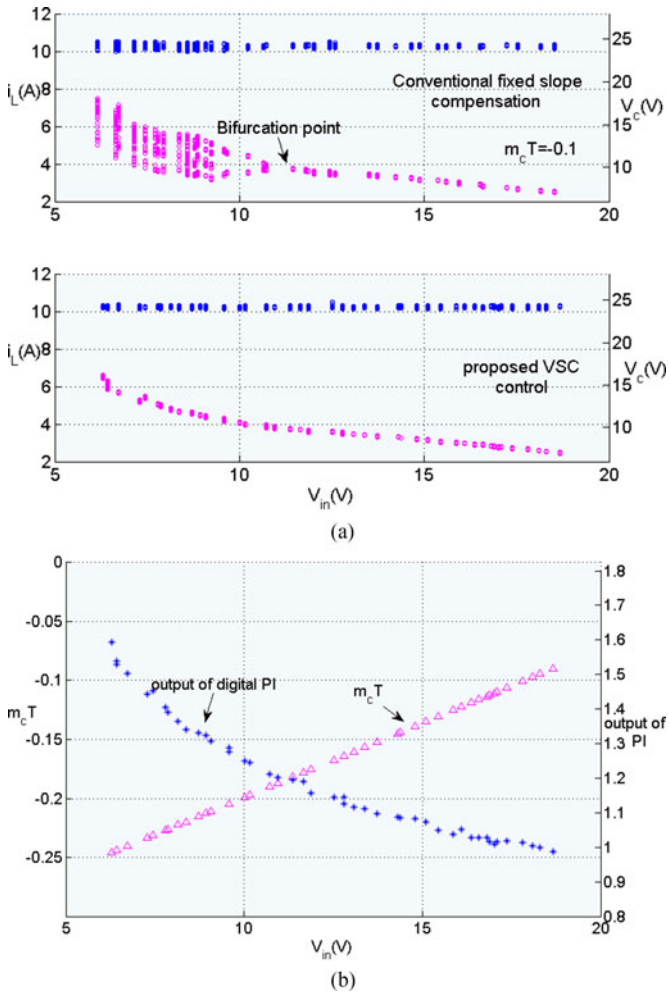

Fig. 14. (a). Comparison of conventional fixed slope compensation and proposed method. (b) Calculated values of mc and output of PI in digital controller.

the following nonlinear transcendental equation can be obtained which should be solved numerically:

$$|\mathrm{eig}(\mathbf{M}(0,T))| = 0.5. \tag{48}$$

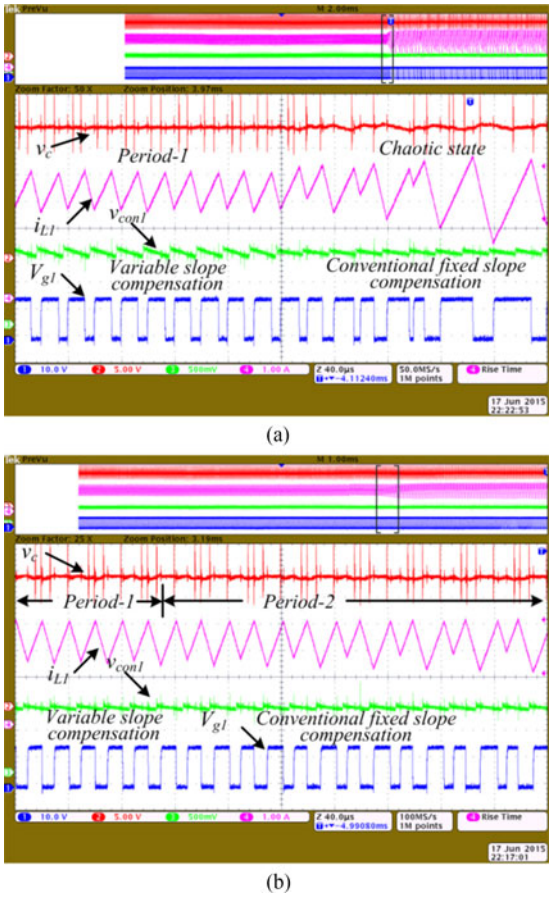

Fig. 15. Control of nonlinearity in converters by employing cycle by cycle VSC: (a) period-1 to chaotic state; and (b) period-1 to period-2.

The relationship of input voltage and the required m_c can be given in the form of a third-order polynomial expression:

$$m_c \cdot T = -2.098 \times 10^{-5} \times V_{\text{in}}^3 + 7.832 \times 10^{-4} \times V_{\text{in}}^2 + 5.5 \times 10^{-3} \times V_{\text{in}} - 0.2561. \quad (49)$$

Fig. 13 shows the polynomial fitting curve and the calculated values of m_c at different input voltages for the given radius of 0.5. Thus, in digital VSC, the amplitudes of the compensation ramp are calculated from the input voltages according to the expression above.

A comparison of conventional fixed slope compensation and the proposed method under digital control is presented in Fig. 14(a). It can be seen that bifurcation occurs when the input voltage is around 11 v with conventional fixed slope compensation; in contrast, the converter remains stable over the whole range of input voltage from 6 to 18 v when employing VCS. Thus, the range of stable operation is effectively extended by using the proposed method. Fig. 14(b) demonstrates the calculated values of $m_c{*}\mathrm{T}$ and the output of digital PI in the operation at different input voltages, which shows that with a linear increase in the absolute value of $m_c{*}\mathrm{T}$, the output of digital PI falls inversely.

Fig. 15 presents the effect of the proposed method on the control of nonlinearity in converters. The waveforms of the output voltage, inductor current, feedback control signals, and gate drives are displayed from the top to the bottom. Fig. 15(a) and (b), respectively, show the moments where the converter loses stability from stable operation of period-1 to the chaotic state and to the period-2. By employing VSC, the system can be kept in stable operation at certain operating conditions; in contrast, when the controller is switched to use conventional fixed slope control, the converter loses stability immediately at one cycle time. Similarly, the system can regain stability by switching to the proposed method within a few time periods of switching cycles. Compared to the stable state, it can also be seen that the ripples of output voltage and inductor current increase remarkably when the converter is in the unstable chaotic state.

VI. Conclusion

The nonlinear phenomenon for an interleaved boost converter is discussed and a new control method based on Monodromy matrix has been presented in this paper. The system dynamic behavior-dependent stability and further understanding of the tipping point for unstable operations can be gained by employing this adopted nonlinear analysis method. This method can be readily extended to other types of dc–dc converters using an interleaving structure. In addition, it provides a new perspective on control laws of designing the appropriate controllers to address the nonlinearities in dc–dc converters. Accordingly, a real-time slope compensation method is proposed to mitigate the nonlinear behavior, which is successfully to extend the range of stable operation and effectively to increase the dynamic robustness by control the nonlinearity as validated by experimental results.

Appendix

The theory of Filippov provides a generalized definition of system solutions with switching behavior [17], [43], [46]. Such systems can be described as

$$\dot{\mathbf{x}}(t) = \begin{cases} f_-(\mathbf{x}(t), t) & \mathbf{x} \in V_- \\ f_\Sigma(\mathbf{x}(t), t) & \mathbf{x} \in \Sigma \\ f_+(\mathbf{x}(t), t) & \mathbf{x} \in V_+ \end{cases} \quad (A1.1)$$

where $f_-(\mathbf{x}(t), t)$ and $f_+(\mathbf{x}(t), t)$ represent the smooth vector fields before and after switching, respectively. V- and V+ are two different regions in state space and the switching manifold Σ separates them, as shown in Fig. A1.1.

In smooth systems, the evaluation of perturbation from the initial condition to the end of the period can be mapped by the fundamental matrix. In nonsmooth systems, however, the switching instant makes the vector field discontinuous. As a result, the fundamental matrix breaks down and the information of the switching instant needs to be taken into account. The relations of perturbation vectors $\Delta\mathbf{x}(t_{\Sigma-})$ and $\Delta\mathbf{x}(t_{\Sigma+})$, which are before and after the switching, respectively, can be described using the saltation matrix

$$\Delta\mathbf{x}(t_{\Sigma+}) = \mathbf{S}\ \Delta\mathbf{x}(t_{\Sigma-}). \quad (A1.2)$$

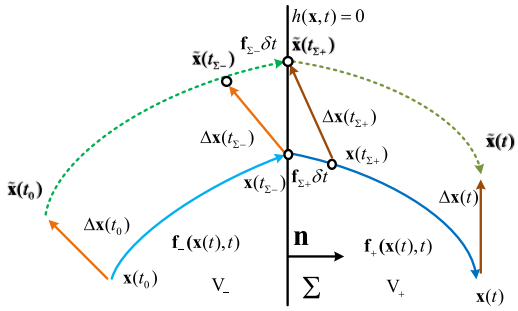

Fig. A1.1 Solution of nonsmooth system and its perturbed solution.

The following equations can be obtained

$$\begin{cases} \Delta\mathbf{x}(t_0) = \tilde{\mathbf{x}}(t_0) - \mathbf{x}(t_0) \\ \Delta\mathbf{x}(t) = \tilde{\mathbf{x}}(t) - \mathbf{x}(t) \\ \tilde{\mathbf{x}}(t_{\Sigma-}) = \mathbf{x}(t_{\Sigma-}) + \Delta\mathbf{x}(t_{\Sigma-}) \\ \tilde{\mathbf{x}}(t_{\Sigma+}) = \mathbf{x}(t_{\Sigma+}) + \Delta\mathbf{x}(t_{\Sigma+}) \\ t_{\Sigma+} = t_{\Sigma-} + \delta t \end{cases}. \tag{A1.3}$$

δt represents the time difference before and after the switching instant, which is small enough. By employing Taylor series expansion, the relationship of the state vectors can be expressed as follows:

$$\tilde{\mathbf{x}}(t_{\Sigma+}) = \tilde{\mathbf{x}}(t_{\Sigma-} + \delta t) = \tilde{\mathbf{x}}(t_{\Sigma-}) + f_{\Sigma-}\delta t \tag{A1.4}$$

$$\mathbf{x}(t_{\Sigma+}) = \mathbf{x}(t_{\Sigma-} + \delta t) = \mathbf{x}(t_{\Sigma-}) + f_{\Sigma+}\delta t. \tag{A1.5}$$

By substituting (A1.4) and (A1.5) into (A1.3), the following is obtained:

$$\begin{aligned} \Delta\mathbf{x}(t_{\Sigma+}) &= \tilde{\mathbf{x}}(t_{\Sigma+}) - \mathbf{x}(t_{\Sigma+}) \\ &= \tilde{\mathbf{x}}(t_{\Sigma-}) - \mathbf{x}(t_{\Sigma-}) + (f_{\Sigma-} - f_{\Sigma+})\delta t. \\ &= \Delta\mathbf{x}(t_{\Sigma-}) + (f_{\Sigma-} - f_{\Sigma+})\delta t \end{aligned} \tag{A1.6}$$

Switching conditions satisfy the following relationship:

$$\begin{cases} h(\mathbf{x}(t_{\Sigma-}), t_{\Sigma-}) = 0 \\ h(\mathbf{x}(t_{\Sigma+}), t_{\Sigma+}) = 0 \end{cases}. \tag{A1.7}$$

Also using the Taylor series expansion on $h(\mathbf{x}(t),t)$, an expression can be derived in terms of δt

$$\begin{aligned} h(\tilde{\mathbf{x}}(t_{\Sigma+}), t_{\Sigma+}) &= h(\mathbf{x}(t_{\Sigma-}) + \Delta\mathbf{x}(t_{\Sigma-}) + f_{\Sigma-}\delta t, t_{\Sigma-} + \delta t) \\ &= \underbrace{h(\mathbf{x}(t_{\Sigma-}), t_{\Sigma-})}_{0} + m\delta t + \mathbf{n}^T(\Delta\mathbf{x}(t_{\Sigma-}) \\ &\quad + f_{\Sigma-}\delta t) = 0 \end{aligned} \tag{A1.8}$$

where

$$\mathbf{n} = \frac{\partial h}{\partial \mathbf{x}}\Big|_{(t_\Sigma, x(t_\Sigma))} \tag{A1.9}$$

and

$$m = \frac{\partial h(\mathbf{x}(t_{\Sigma-}), t_{\Sigma-})}{\partial t} = \frac{\partial h(\mathbf{x}(dT), dT)}{\partial t} = \frac{\partial h}{\partial t}\Big|_{x(dT), dT}. \tag{A1.10}$$

Here, $\mathbf{n}$ represents the normal to the switching manifold. The expression for δt can be obtained as

$$\delta t = -\frac{\mathbf{n}^T \Delta\mathbf{x}(t_{\Sigma-})}{\mathbf{n}^T f_{\Sigma-} + m}. \tag{A1.11}$$

Substituting (A1.8), (A1.9), and (A1.10) into (A1.11), the relationship between the perturbations vectors before and after the switching is shown as

$$\Delta\mathbf{x}(t_{\Sigma+}) = \Delta\mathbf{x}(t_{\Sigma-}) + (f_{\Sigma+} - f_{\Sigma-})\frac{\mathbf{n}^T \Delta\mathbf{x}(t_{\Sigma-})}{\mathbf{n}^T f_{\Sigma-} + m}. \tag{A1.12}$$

Comparing (A1.2) and (A1.12), the saltation matrix can be written as

$$\mathbf{S} = \mathbf{I} + \frac{(f_{\Sigma+} - f_{\Sigma-})\mathbf{n}^T}{\mathbf{n}^T f_{\Sigma-} + \frac{\partial h}{\partial t}}. \tag{A1.13}$$

REFERENCES

[1] T. Jiun-Ren, W. Tsai-Fu, W. Chang-Yu, C. Yaow-Ming, and L. Ming-Chuan, "Interleaving phase shifters for critical-mode boost PFC," *IEEE Trans. Power Electron.*, vol. 23, no. 3, pp. 1348–1357, May 2008.

[2] L. Wuhua and H. Xiangning, "A family of isolated interleaved boost and buck converters with winding-cross-coupled inductors," *IEEE Trans. Power Electron.*, vol. 23, no. 6, pp. 3164–3173, Nov. 2008.

[3] K. Dong-Hee, C. Gyu-Yeong, and L. Byoung-Kuk, "DCM analysis and inductance design method of interleaved boost converters," *IEEE Trans. Power Electron.*, vol. 28, no. 10, pp. 4700–4711, Oct. 2013.

[4] O. Hegazy, J. Van Mierlo, and P. Lataire, "Analysis, modeling, and implementation of a multidevice interleaved DC/DC converter for fuel cell hybrid electric vehicles," *IEEE Trans. Power Electron.*, vol. 27, no. 11, pp. 4445–4458, Nov. 2012.

[5] J. Doo-Yong, J. Young-Hyok, P. Sang-Hoon, J. Yong-Chae, and W. Chung-Yuen, "Interleaved Soft-Switching boost converter for photovoltaic Power-Generation system," *IEEE Trans. Power Electron.*, vol. 26, no. 4, pp. 1137–1145, Apr. 2011.

[6] N. Long-xian, S. Kai, Z. Li, X. Yan, C. Min, and L. Rosendahl, "A power conditioning system for thermoelectric generator based on interleaved Boost converter with MPPT control," in *Proc. 2011 Int. Conf. Elect. Mach. Syst.*, 2011, pp. 1–6.

[7] Y. Chen, C. K. Tse, S. C. Wong, and S. S. Qiu, "Interaction of fast-scale and slow-scale bifurcations in current-mode controlled dc/dc converters," *Int. J. Bifurcation Chaos*, vol. 17, pp. 1609–1622, May 2007.

[8] D. Giaouris, S. Banerjee, O. Imrayed, K. Mandal, B. Zahawi, and V. Pickert, "Complex interaction between tori and onset of Three-Frequency Quasi-Periodicity in a current mode controlled boost converter," *IEEE Trans. Circuits Syst. I, Reg. Papers*, vol. 59, no. 1, pp. 207–214, Jan. 2012.

[9] H. H. C. Lu and C. K. Tse, "Study of low-frequency bifurcation phenomena of a parallel-connected boost converter system via simple averaged models," *IEEE Trans. Circuits Syst. I, Fundam. Theory Appl.*, vol. 50, no. 5, pp. 679–686, May 2003.

[10] P. T. Krein, J. Bentsman, R. M. Bass, and B. C. Lesieutre, "On the use of averaging for the analysis of power electronic systems," *IEEE Trans. Power Electron.*, vol. 5, no. 2, pp. 182–190, Apr. 1990.

[11] B. Lehman and R. M. Bass, "Switching frequency dependent averaged models for PWM DC-DC converters," *IEEE Trans. Power Electron.*, vol. 11, no. 1, pp. 89–98, Jan. 1996.

[12] V. A. Caliskan, G. C. Verghese, and A. M. Stankovic, "Multifrequency averaging of DC/DC converters," *IEEE Trans. Power Electron.*, vol. 14, no. 1, pp. 124–133, Jan. 1999.

[13] S. R. Sanders, J. M. Noworolski, X. Z. Liu, and G. C. Verghese, "Generalized averaging method for power conversion circuits," *IEEE Trans. Power Electron.*, vol. 6, no. 2, pp. 251–259, Apr. 1991.

[14] S. Jian and R. M. Bass, "A new approach to averaged modeling of PWM converters with current-mode control," in *Proc. 23rd Int. Conf. Ind. Electron., Control Instrum.*, 1997, vol. 2, pp. 599–604.

[15] M. di Bernardo and F. Vasca, "Discrete-time maps for the analysis of bifurcations and chaos in DC/DC converters," *IEEE Trans. Circuits Syst. I, Reg. Papers*, vol. 47, no. 2, pp. 130–143, Feb. 2000.
[16] S. Almer, U. Jonsson, C. Y. Kao, and J. Mari, "Global stability analysis of DC-DC converters using sampled-data modeling," in *Proc. 2004 Amer. Control Conf.*, 2004, vol. 1–6, pp. 4549–4554.
[17] D. Giaouris, S. Banerjee, B. Zahawi, and V. Pickert, "Stability analysis of the continuous-conduction-mode buck converter via Filippov's method," *IEEE Trans. Circuits Syst. I, Reg. Papers*, vol. 55, no. 4, pp. 1084–1096, May 2008.
[18] S. K. Mazumder and K. Acharya, "Multiple Lyapunov function based reaching condition for orbital existence of switching power converters," *IEEE Trans. Power Electron.*, vol. 23, no. 3, pp. 1449–1471, May 2008.
[19] I. A. Hiskens and M. A. Pai, "Trajectory sensitivity analysis of hybrid systems," *IEEE Trans. Circuits Syst. I, Reg. Papers*, vol. 47, no. 2, pp. 204–220, Feb. 2000.
[20] E. Rodriguez, A. El Aroudi, F. Guinjoan, and E. Alarcon, "A ripple-based design-oriented approach for predicting fast-scale instability in DC-DC switching power supplies," *IEEE Trans. Circuits Syst. I, Reg. Papers*, vol. 59, no. 1, pp. 215–227, Jan. 2012.
[21] A. El Aroudi, E. Rodriguez, R. Leyva, and E. Alarcon, "A design-oriented combined approach for bifurcation prediction in switched-mode power converters," *IEEE Trans. Circuits Syst. II, Express Briefs*, vol. 57, no. 3, pp. 218–222, Mar. 2010.
[22] K. Mehran, D. Giaouris, and B. Zahawi, "Stability analysis and control of nonlinear phenomena in boost converters using model-based Takagi–Sugeno fuzzy approach," *IEEE Trans. Circuits Syst. I, Reg. Papers*, vol. 57, no. 1, pp. 200–212, Jan. 2010.
[23] K. H. Wong, "Output capacitor stability study on a voltage-mode buck regulator using system-poles approach," *IEEE Trans. Circuits Syst. II, Express Briefs*, vol. 51, no. 8, pp. 436–441, Aug. 2004.
[24] X. M. Wang, B. Zhang, and D. Y. Qiu, "The quantitative characterization of symbolic series of a boost converter," *IEEE Trans. Power Electron.*, vol. 26, no. 8, pp. 2101–2105, Aug. 2011.
[25] N. Quanmin, J. Zhizhong, Q. Chengchao, and W. Hengli, "Study on bifurcation and chaos in boost converter based on energy balance model," in *Proc. Asia-Pacific Power Energy Eng. Conf.*, 2009, pp. 1–5.
[26] A. El Aroudi, D. Giaouris, H. Ho-Ching Iu, and I. A. Hiskens, "A review on stability analysis methods for switching mode power converters," *IEEE J. Emerg. Sel. Topics Circuits Syst.*, vol. 5, no. 3, pp. 302–315, Sep. 2015.
[27] E. Ott, C. Grebogi, and J. A. Yorke, "Controlling chaos," *Phys. Rev. Lett.*, vol. 64, 1990, Art. no. 1196.
[28] R. S. Bueno and J. L. R. Marrero, "Application of the OGY method to the control of chaotic DC-DC converters: Theory and experiments," in *Proc. IEEE Int. Symp. Circuits Syst.*, 2000, pp. 369–372.
[29] A. Y. Goharrizi, A. Khaki-Sedigh, and N. Sepehri, "Observer-based adaptive control of chaos in nonlinear discrete-time systems using time-delayed state feedback," *Chaos Solitons Fractals*, vol. 41, pp. 2448–2455, Sep. 15, 2009.
[30] N. Wang, G. N. Lu, X. Z. Peng, and Y. K. Cai, "A research on time delay feedback control performance in chaotic system of DC-DC inverter," in *Proc. 2013 IEEE Int. Conf. Veh. Electron. Safety*, 2013, pp. 215–218.
[31] W. Ma, M. Y. Wang, S. X. Liu, S. Li, and P. Yu, "Stabilizing the average-current-mode-controlled boost PFC converter via washout-filter-aided method," *IEEE Trans. Circuits Syst. II, Express Briefs*, vol. 58, no. 9, pp. 595–599, Sep. 2011.
[32] A. El Aroudi, R. Haroun, A. Cid-Pastor, and L. Martinez-Salamero, "Suppression of line frequency instabilities in PFC AC-DC power supplies by feedback notch filtering the pre-regulator output voltage," *IEEE Trans. Circuits Syst. I, Reg. Papers*, vol. 60, no. 3, pp. 796–809, 2013.
[33] L. Wei-Guo, Z. Luo-Wei, and W. Jun-Ke, "Self-stable chaos control of dc–dc converter," *Chinese Phys. Lett.*, vol. 26, 2009, Art. no. 030503.
[34] J. Xu, G. Zhou, and M. He, "Improved digital peak voltage predictive control for switching DC–DC converters," *IEEE Trans. Ind. Electron.*, vol. 56, no. 8, pp. 3222–3229, Aug. 2009.
[35] E. Rodriguez, E. Alarcon, H. H. C. Iu, and A. El Aroudi, "A frequency domain approach for controlling chaos in switching converters," in *Proc. 2010 IEEE Int. Symp. Circuits Syst.*, 2010, pp. 2928–2931.
[36] Y. F. Zhou, H. H. C. Iu, C. K. Tse, and J. N. Chen, "Controlling chaos in DC/DC converters using optimal resonant parametric perturbation," in *Proc. 2005 IEEE Int. Symp. Circuits Syst.*, 2005, pp. 2481–2484.
[37] Y. Zhou, C. K. Tse, S.-S. Qiu, and F. C. M. Lau, "Applying resonant parametric perturbation to control chaos in the buck dc/dc converter with phase shift and frequency mismatch considerations," *Int. J. Bifurcation Chaos*, vol. 13, pp. 3459–3471, 2003.
[38] B. Bocheng, Z. Guohua, X. Jianping, and L. Zhong, "Unified classification of operation-state regions for switching converters with ramp compensation," *IEEE Trans. Power Electron.*, vol. 26, no. 7, pp. 1968–1975, Jul. 2011.
[39] N. Inaba, T. Endo, T. Yoshinaga, and K. Fujimoto, "Collapse of mixed-mode oscillations and chaos in the extended Bonhoeffer-van Der pol oscillator under weak periodic perturbation," in *Proc. 2011 20th Eur. Conf. Circuit Theory Design*, 2011, pp. 369–372.
[40] K. Guesmi, A. Hamzaoui, and J. Zaytoon, "Control of nonlinear phenomena in DC–DC converters: Fuzzy logic approach," *Int. J. Circuit Theory Appl.*, vol. 36, pp. 857–874, 2008.
[41] H. Wu, V. Pickert, and D. Giaouris, "Nonlinear analysis for interleaved boost converters based on Monodromy matrix," in *Proc. 2014 IEEE Energy Convers. Congr. Expo.*, 2014, pp. 2511–2516.
[42] H. Wu and V. Pickert, "Stability analysis and control of nonlinear phenomena in bidirectional boost converter based on the Monodromy matrix," in *Proc. 2014 29th Annu. IEEE Appl. Power Electron. Conf. Expo.*, 2014, pp. 2822–2827.
[43] R. I. Leine and H. Nijmeijer, *Dynamics and Bifurcations of Non-Smooth Mechanical Systems*, vol. 18. New York, NY, USA: Springer, 2013.
[44] M. Hallworth and S. A. Shirsavar, "Microcontroller-based peak current mode control using digital slope compensation," *IEEE Trans. Power Electron.*, vol. 27, no. 7, pp. 3340–3351, Jul. 2012.
[45] S. Chattopadhyay and S. Das, "A digital current-mode control technique For DC–DC converters," *IEEE Trans. Power Electron.*, vol. 21, no. 6, pp. 1718–1726, Nov. 2006.
[46] A. O. Elbkosh, "Nonlinear analysis and control of DC-DC converters," Ph.D. thesis, Newcastle University, Newcastle upon Tyn, U.K., 2009.

Haimeng Wu (M'10) was born in Zhejiang, China, in 1986. He received the B.Sc. degree in electrical engineering from Chongqing University, Chongqing, China, in 2008. He was nominated as the postgraduate exempted from the national postgraduate entrance examination to Zhejiang University, and then he received the M.Sc. degree in power electronics from the College of Electrical Engineering, Zhejiang University, Hangzhou, China, in 2011. He received the grants from Engineering and Physical Science Council for his further education in U.K. He received the Ph.D. degree in power electronics from the School of Electrical and Electronic Engineering, Newcastle University, U.K., in 2016.

He has been with the Electrical Power Research Group at Newcastle University as a Postdoctoral Researcher since 2015. His current research interests include power electronics for electric vehicles and advanced nonlinear control.

Volker Pickert (M'04) studied electrical and electronic engineering at the Rheinisch–Westfaelische Technische Hochschule (RWTH), Aachen, Germany and Cambridge University, Cambridge, U.K. He received the Dipl.-Ing. degree in electrical and electronic engineering from RWTH in 1994 and the Ph.D. degree in power electronics from Newcastle University, Newcastle upon Tyne, U.K., in 1997.

From 1998 to 1999, he was an Application Engineer with Semikron GmbH, Nuremberg, Germany and from 1999 to 2003 he was a Group Leader at Volkswagen AG, Wolfsburg, Germany, responsible for the development of electric drives for electric vehicles. In 2003, he was appointed as a Senior Lecturer in the Electrical Power Research Group, Newcastle University and in 2011 he became a Full Professor of power electronics. In 2012, he became the Head of the Electrical Power Research Group. He has published more than 120 book chapters, journal, and conference papers in the area of power electronics and electric drives. His current research interests include power electronics for automotive applications, thermal management, health monitoring techniques, and advanced nonlinear control.

Prof. Pickert received the IMarEST Denny Medal for the best article in the *Journal of Marine Engineering* in 2011. He was the Chairman of the biannual international IET conference on Power Electronics, Machines and Drives in 2010 in Brighton and he is the active Editor-in-Chief of the *IET Power Electronics* Journal.

Damian Giaouris (M'04) received the B.Sc. degree in mathematics from Open University, Milton Keynes, U.K., in 2009, the B.Eng. degree in automation engineering from Technological Educational Institute of Thessaloniki, Sindos, Greece, in 2000, the Postgraduate Certificate in mathematics from Open University, in 2011, and the Ph.D. and M.Sc. degrees in the area of control of electrical systems from Newcastle University, Newcastle upon Tyne, U.K., in 2004 and 2001, respectively.

He was a Lecturer in control systems at Newcastle University since 2004, before moving to the Centre for Research and Technology Hellas, Greece, in 2011. Since September 2015, he is a Senior Lecturer of control of electrical systems at Newcastle University. His research interests include control of power converters, power systems, smart grids, electric vehicles, and nonlinear dynamics of electrical systems. He has more than 115 publications (with more than 1400 citations).

Dr. Giaouris is currently an Associate Editor of *IET Power Electronics* and has been a Guest Associate Editor of the IEEE JOURNAL ON EMERGING AND SELECTED TOPICS IN CIRCUITS AND SYSTEMS.

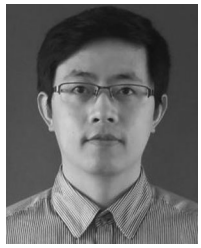

Bing Ji (M'13) received the M.Sc. and Ph.D. degrees in electrical and electronic engineering from Newcastle University, Newcastle upon Tyne, U.K., in 2007 and 2012, respectively.

Since 2012, he has been with the electrical powertrain and battery management systems of electric vehicles as a Power Electronics Engineer with a U.K.'s low-emission vehicle company. He joined Newcastle University as a Postdoctoral Researcher, in 2013, working on accurate power loss measurement and health management for power electronics. He is currently a Lecturer of electrical power engineering with the University of Leicester, Leicester, U.K. His research interests include reliability of power semiconductor devices, batteries and converters, function integration of gate drivers, electrothermal modeling, thermal management, and high power-density converter integration for electric vehicle applications.

Dr. Ji is also a Member of the IET.